

Light propagation in pulp and paper research

Heidi Brunborg*, Torbjørn Smørgrav,† Richard Blake,‡ Per Nygård§
NTNU, IME
Department of computer
and information science

Abstract

A new solution for light simulation using forward ray tracing is presented. Aiming to archive statically right physical resemblance, the framework is trying hard to be faithful to the physics of light and its interaction with matter. The complexity of the system is controlled by dividing the sphere around each scattering event into discrete patches, grouping the irradiance into these patches. A ray represent one patch with radiant intensity. Phenomena incorporated are reflection, refraction, dispersion, absorption and subsurface scattering.

A proof of concept is implemented in C++, and a simple deterministic scene descriptions with point light source and a copper sphere serves as test cases. The input is given with XML files and the output is post processed into nonuniform polar plots.

The results are few but promising. Some aspects of the underlying physics needs to be refined and yet to be answered is how the system will respond to a complex scene description.

1 Universe Representation

There are many ways to represent a simulation universe. The complex structure of paper sheets can be represented in at least three different ways.

The most common parameterization in ray tracing is the deterministic model from synthesis. The paper is explicitly described with primitives. Examples of primitives used is cylinder (fiber) and ellipsoid (pore). These primitives have a fixed position and orientation in the universe.

*heidibr@stud.ntnu.no

†torbjorn@smorgrav.org

‡blake@idi.ntnu.no

§per.nygard@pfi.no

A deterministic representation from acquisition of the complex structure is also possible. An example would be data acquired at the European Synchrotron Radiation Facility, see [1] for further details. This type of universe would also be fixed, but the shape of components would be “exact” copies of real objects rather than primitives.

The complex structure may also be represented statistically. In this option the universe is described by statistical knowledge of the shape, behavior and density of universe primitives. The light simulation program, Grace [2], used this type of parameterization. Distributions describing the probability of hitting a certain type of component at a certain position in the universe is an example of input to a statistically parameterized universe.

The two most important constructs in the raytracer developed are ray and component. The ray has wavelength and radiant intensity. Any type of matter/media that a ray may interact with in our model-universe will be a component. Anything that consists of non-magnetic matter and gases can be modeled. At least this is true as long as it can be sufficiently defined by the attributes of a component, which are the following:

- shape
- surface roughness (microfacet distribution)
- absorption spectrum $\alpha(\lambda)$
- reflection values $r(\lambda, \theta_i)$
- refraction indices $\hat{N}(\lambda)$

2 Physical Foundation

The raytracer developed is physically based. The equation describing a wave propagating in matter

(Equation 1), is derived from Maxwell's equations[3].

$$E(\mathbf{r}, t) = E_0 \exp \left\{ i\omega \left(\frac{n}{c} \mathbf{n}_q \cdot \mathbf{r} - \mathbf{t} \right) \right\} \exp \left\{ -\frac{\omega k}{c} \mathbf{n}_q \cdot \mathbf{r} \right\} \quad (1)$$

The first exponent of the equation describes the fact that the velocity of light (phase velocity) is reduced from its value in free space, c , to c/n . The second exponent gives the damping of the wave. The amplitudes of the fields are reduced by $\exp \{-2\pi k/n\}$ per wavelength λ in the medium. This can describe the attenuation of the light intensity $I(r) = I_0 \exp \{-\alpha r\}$ propagating in a medium (Equation 2).

$$\alpha = \frac{2k\omega}{c} = \frac{4\pi k}{\lambda_0} \quad (2)$$

Hence the absorption ratio, α , of a ray in a component is given by the wavelength of the ray and the extinction coefficient k .

The extinction coefficient is the imaginary part of the complex refractive index. The complex refractive index describes the optical properties of a component and is given by Equation 3.

$$\hat{N} = n - ik = \left[\varepsilon_1 \mu_1 + i \frac{4\pi \mu_1 \sigma_1}{\omega} \right]^{1/2} \quad (3)$$

The real part, n is related to the velocity. Refractive indices are different for different wavelengths, so we need to know the \hat{N} of matter as a function of wavelengths. Such functions are generally not known, but there exist experimentally measured reflection-ratios for several materials [4].

When light is incident on matter a ratio of the the intensity will reflect from the medium and the remaining intensity will refract into the medium. Reflection and refraction ratios are given by the Fresnel formulas.

These formulas are given for two different cases, depending on the polarization of the incident light. Equation 4 and 5 give the parallel (\hat{t}_{\parallel}) and perpendicularly (\hat{t}_{\perp}) polarized transmission (refraction) ratios, while Equation 6 and 7 give the corresponding reflection ratios. For unpolarized light the relative magnitude is the average of the two formulas, Equation 8 and Equation 9. These equations are valid for the interface between vacuum and matter. To make it more general, substitute \hat{N} with \hat{N}/\hat{N}' and μ_1 with μ_1/μ_1' . Where \hat{N}' and μ_1' are the properties of the medium the wave comes from.

$$\hat{t}_{\perp} = \frac{E_{0t}}{E_{0i}} = \frac{2\mu_1 \cos \psi_i}{\mu_1 \cos \psi_i + \sqrt{\hat{N}^2 - \sin^2 \psi_i}} \quad (4)$$

$$\hat{t}_{\parallel} = \frac{E_{0t}}{E_{0i}} = \frac{2\mu_1 \hat{N} \cos \psi_i}{\hat{N}^2 \cos \psi_i + \mu_1 \sqrt{\hat{N}^2 - \sin^2 \psi_i}} \quad (5)$$

$$\hat{r}_{\perp} = \frac{E_{0r}}{E_{0i}} = \frac{\mu_1 \cos \psi_i - \sqrt{\hat{N}^2 - \sin^2 \psi_i}}{\mu_1 \cos \psi_i + \sqrt{\hat{N}^2 - \sin^2 \psi_i}} \quad (6)$$

$$\hat{r}_{\parallel} = \frac{E_{0r}}{E_{0i}} = \frac{\hat{N}^2 \cos \psi_i - \mu_1 \sqrt{\hat{N}^2 - \sin^2 \psi_i}}{\hat{N}^2 \cos \psi_i + \mu_1 \sqrt{\hat{N}^2 - \sin^2 \psi_i}} \quad (7)$$

$$\hat{t} = \frac{\hat{t}_{\perp} + \hat{t}_{\parallel}}{2} \quad (8)$$

$$\hat{r} = \frac{\hat{r}_{\perp} + \hat{r}_{\parallel}}{2} \quad (9)$$

Since the refractive index is wavelength dependent, we see that the Fresnel formulas are both wavelength (λ) and incident angle (ψ_i) dependent.

The specular direction of the refracted intensity is given by the well known Snell's law:

$$\frac{\sin \psi_i}{\sin \psi_t} = \frac{\hat{N}_t}{\hat{N}_i} \quad (10)$$

2.1 Surface Scattering

The incident light is neither reflected nor refracted purely in the specular direction. This phenomena is due to surface roughness where microfacet orientations deviate from the surface normal of the component. The reflection due to light hitting these microfacets is called surface scattering. The microfacet orientations can be described by distributions like the Beckmann or the Gaussian distributions. Cook and Torrance were the first to introduce microfacet distributions to illumination models [5]. The root mean square (rms) of the facet orientations can be measured using an atomic force microscope The Beckmann distribution is a function depends on the rms of the surface. The Beckmann function is given in Equation 11, where m is the rms.

$$D(\theta_i) = \frac{1}{4m^2 \cos^2 \theta_i} e^{-[\tan \theta/m]^2} \quad (11)$$

2.2 Subsurface Scattering

Diffuse scattering may be due to microfacets or due to scattering subsurface. On its way through matter, light will continue in its original direction or scatter in new directions due to several phenomena of which some will be listed in the following.

- If the wave (photon) is absorbed and re-emitted, the emitted direction is random and the wavelength may be shifted by Compton's shift formula. In this work, we only consider coherent scattering, i.e. scattering for which reemission occurs at the same frequency as the incident radiation.
- If the wave "hits" a particle that is smaller than the wavelength, the predominant mode of scattering is elastic (no energy loss or phase shift) scattering, called Rayleigh scattering (Equation 12). This scattering is responsible for the blue color of the sky; it increases with the fourth power of the frequency and is more effective at short wavelengths (Equation 13). It occurs mostly in gases, transparent solids and crystalline structures.

$$I = I_0 \frac{8\pi_4 N \alpha^2}{\lambda^4 R^2} (1 + \cos^2 \theta^2) \quad (12)$$

$$I \rightarrow \frac{I}{\lambda^4} \quad (13)$$

- For particles larger than the wavelengths, the scattering is predominant by a phase function expressed by the Mie scattering. Mie is also elastic scattering that occurs in gas and transparent solids. A comparison of Mie and Rayleigh is illustrated in Figure 1.
- Brillouin scattering is scattering from acoustic modes. From a strictly classical point of view, the compression of the medium will change the index of refraction and therefore lead to some reflection or scattering at any point where the index changes. Brillouin scattering is typically shifted by 0.1 to 1 cm^{-1} from the incident light.
- Light that is scattered due to vibrations in molecules or optical phonons in solids is called Raman scattering. Raman scattered light is shifted by as much as 4000 cm^{-1} from the incident light. Raman scattering occurs in solids.

On a more abstract level, photons travel between successive scattering events whose cumulative effect is to produce a random walk. Similar multiple scattering processes occur for photons in astrophysical structures, electrons and phonons in solids, neutrons in reactors, and molecules in a gas. The mean free path is the mean length (steplength) to next scattering event. A combination of the two scattering phenomena Mie and Rayleigh is expressed in the Henyey-Greenstein

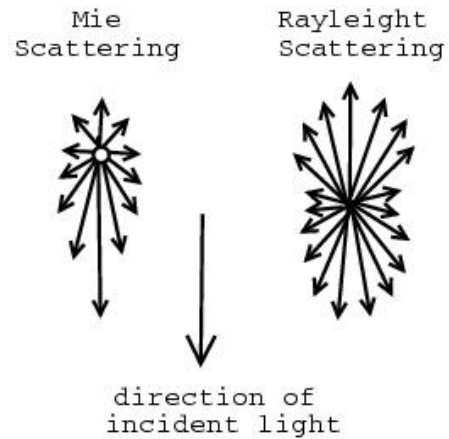


Figure 1: The difference between Rayleigh and Mie scattering

phase function. It was first introduced by Henyey and Greenstein (1941) to describe scattering of radiation in a galaxy. The Henyey-Greenstein phase function is often used to characterize the angular distribution of scattered light by tissue and cellulose [6] and is characterized by the average cosine, g , of the scattering angle, j , (Equation 14).

$$PHG(\cos j) = \frac{1}{4\pi} \frac{1 - g^2}{(1 + g^2 - 2g \cos j)^{3/2}} \quad (14)$$

All scattering happening due to the two phenomena listed above will be called subsurface scattering in the light propagation model described in the following section of this article.

3 The Light Propagation Model - LPM

The development of a light simulation model aimed at simulation on complex structures for the pulp and paper community has emphasized physical correctness of the light propagation. Physical properties of light and matter is very complex and may be described at several levels of detail. This simulation model organizes the propagation of light into the two types of scattering events mentioned in the previous section. The life of a ray in the Light Propagation Model developed and the conservation of energy in this model will now be described.

3.1 Life cycle of a ray

Figure 2 illustrates the life cycle of a ray. The figure contains two interfaces with a ray starting at the upper interface and ending on the lower interface. The

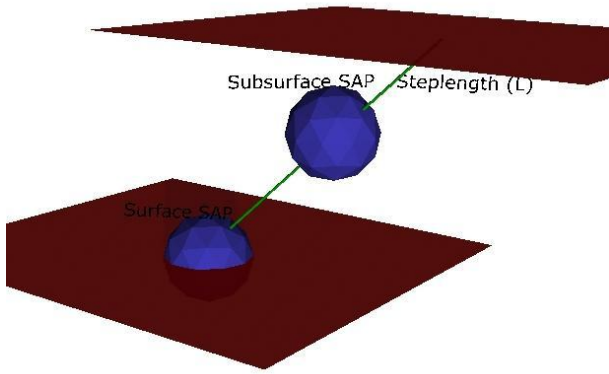


Figure 2: A ray and the two scattering events from start, through a medium and to the ray ends at the interface of the next medium.

space between the two interfaces is the inside of one component. During its journey from one interface to the next, the ray encounters two events modeled by a subsurface scattering and a surface scattering. These scattering events are realized through the Sphere Area Partitioning (SAP) concept explained in Section 3.3. A subsurface scattering happens after a steplength l where a ratio σ of the ray is scattered. The scattered intensity makes new rays with intensities and directions according to the subsurface SAP. The new rays are queued while the rest of the original ray continues to the next interface. All propagation causes attenuation according to travel length and absorption ratio α . On the next interface, i.e. the surface of the current component, a new scattering event occurs. As for the subsurface scattering event, a surface SAP provides the intensity and direction of all new rays made by this event. Unlike subsurface scattering, all intensity is scattered and the original ray vanishes. A ray only exists in one component and only has one direction during its lifetime. The intensity of a ray scattered into new directions during a scattering event is defined as new rays, ready to go through the same life cycle. Figure 3 illustrates the life of a ray in two dimensions while Figure 2 illustrated the same in 3D.

3.2 Algorithm

We are now ready to gain a better understanding of the the whole process of one ray becoming a set of new rays. Two sets of equations are presented which describes the change of the electric field of a ray during its lifetime in the LPM.

Equations 15 through 19 represent the general continuity equation.

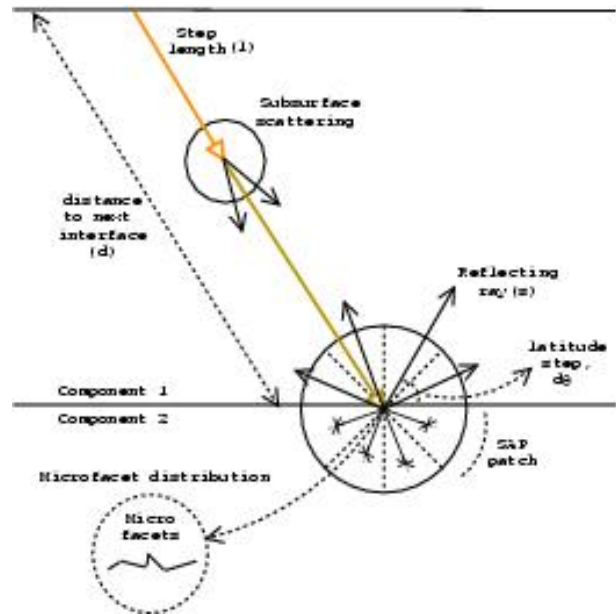


Figure 3: A cross-section of the scattering-events in the life of a ray as modeled in LPM.

$$E_0 = E_0 \alpha l \tag{15}$$

$$+ E_0 (1 - \alpha l) \sigma \tag{16}$$

$$+ E_0 (1 - \alpha l) (1 - \sigma) \alpha d \tag{17}$$

$$+ E_0 (1 - \alpha l) (1 - \sigma) (1 - \alpha d) r \tag{18}$$

$$+ E_0 (1 - \alpha l) (1 - \sigma) (1 - \alpha d) \bar{r} \tag{19}$$

- The first phenomena to account for is attenuation as the ray moves in the medium (Equation 15). E_0 is the incident light, α is the absorption coefficient of the component and l is the distance the ray travels in the medium. What is left of the ray after event one is $E_0(1 - \alpha l)$.
- The remaining part of the ray is subsurface scattered (Equation 16). σ is the ratio of the field to be scattered. Now after event one and two $E_0(1 - \alpha l)(1 - \sigma)$ is left of the original ray.
- The rest of the ray goes straight through the component to the interface with another medium. The ray attenuates during this distance d according to the absorption coefficient α (Equation 17).
- On the interface, one part reflects back into the medium it came from with reflection coefficient r (Equation 18).
- The other part ($\bar{r} = 1 - r$), refracts into the new

medium (Equation 19). $\bar{r} + r = 1$ is always true in LPM.

The electric field in subsurface scattering (Equation 16), reflection (Equation 18) and refraction (Equation 19) may scatter in every possible direction of the continuous sphere surrounding the scattering point. Therefore these equations can be represented by surface integral over the sphere surrounding the scattering point, but continuous integration is not well suited for implementation. To control the complexity of the simulation or growth of rays the continuous sphere is divided into discrete patches, where each patch (ω) will be represented by one ray with direction equal to the normal of the patch centerpoint and with intensity equal to the grouped intensity of the patch. By increasing the number of rays, i.e. decreasing the patch area, this model should become increasingly accurate. This situation is described by Equations 20 through 22.

$$\sum_0^{|\omega|} E_{s(\omega)} = E_0(1 - \alpha l)\sigma \quad (20)$$

$$\sum_0^{|\omega|} E_{r(\omega)} = E_0(1 - \alpha l)(1 - \sigma)(1 - \alpha d)r \quad (21)$$

$$\sum_0^{|\omega|} E_{\bar{r}(\omega)} = E_0(1 - \alpha l)(1 - \sigma)(1 - \alpha d)\bar{r} \quad (22)$$

This sphere around each scattering point will have to scatter according to the surface and subsurface distributions. The Sphere Area Partitioning (SAP) concept was developed to take care of this behaviour. The working of a SAP will be explained in the following section.

3.3 Sphere Area Partitioning

In addition to being faithful to the physics of light, the strength of this simulation framework is its ability to control complexity through the SAP concept. Two important issues of the SAP are the method used for dividing the sphere into equal-sized patches and the population of reflection ratios into each patch.

3.3.1 Tessellation

Hierarchical, equal area and iso-latitude pixelisation is the method used for partitioning the sphere. This method, HEALPix is developed by a group under The European Southern Observatory [7]. The following

properties will be fulfilled when tessellating a SAP with the HEALPix technique:

1. Each scattering direction is mapped to one patch only.
2. The average of all directions intersecting a patch is equal to the normal direction at the center of the patch. The direction of a ray scattered through a patch should be set equal to this normal.
3. The granularity of the tessellation is easy to adjust.
4. Each patch is easy to access.
5. It is easy to find the area and the boundary of each patch.
6. The tessellation results in patches with equal area.

The possibility to run the simulation with different number of patches on a sphere will provide a strong mean to control the complexity of the simulation.

3.3.2 Populating the SAP

Each patch in a SAP will hold a ratio giving the fraction of incident intensity that will be reflected in this patch. The act of distributing ratios to the patches will be referred to as populating a SAP. This population should be based on knowledge about the scattering phenomena in question. For surface scattering events, the microfacet distribution of the surface will guide the population. In the case of subsurface scattering, a phase-function like the Henyey-Greenstein equation may be used for the population [8]. Both types of scattering may also be populated by standard distributions like the Gaussian and exponential distributions.

The scattering events are three dimensional, hence volumetric distributions integrating to one is needed. The Facet Model in [9] provides an equation for calculating the facet slope ζ , of a microfacet given incident angle and reflection direction, see Equation 23. The polar incident angle is given by θ_i , whereas (θ_p, ϕ_p) represent the direction of a patch.

$$\zeta = \frac{\sqrt{\sin^2(\theta_i) - 2\sin(\theta_i)\sin(\theta_p)\cos(\phi_p) + \sin^2(\theta_p)}}{\cos(\theta_i) + \cos(\theta_p)} \quad (23)$$

When the facet slopes corresponding to the patches of the SAP are calculated, the ratio corresponding to the slopes can be found by Equation 24, where h is the

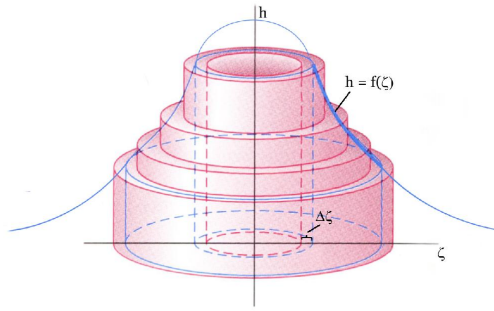


Figure 4: The volume of a cylinder, $p(\zeta)$, represents the probability of a certain facet slope interval of the distribution given by $f(\zeta)$.

height of the microfacet distribution at ζ . Example of a Gaussian facet slope distribution is given in Equation 25. Figure 3.3.2 illustrates a 3D distribution of the facet slopes.

$$p(\zeta) = 2\pi\zeta h \Delta\zeta \tag{24}$$

As seen from Figure 3.3.2 is the probability of a certain facet slope interval given by the volume of a cylinder given in Equation 24, where the height of the cylinder, h , is given by a microfacet distribution. The microfacet distribution given as an example in Equation 25, is the Gaussian distribution used by the Scatmech library [10]. σ is the standard deviation of the distribution, which will decide the degree of diffuse scattering.

$$f(\zeta) = \frac{1}{\pi \cdot \sigma^2} \exp\left(-\left(\frac{\zeta}{\sigma}\right)^2\right) \tag{25}$$

3.3.3 Rotating the SAP

When a SAP has been populated it is ready to be used by scattering events happening on the surface or in the matter it represents. Though the ratios of the SAP decides how specular or diffuse the scattering is, the distribution will always be centered around the specular reflection, refraction, forward or backward scattering direction. A SAP is populated according to normal incidence and for every scattering event the SAP will be rotated according to the current incident angle.

4 Simulation

This section aims to verify the LPM and the implementation of the model, named LightPro. The only implemented parameterization available is the deterministic type. Thus the test scene is a deterministic

defined scene with a lightsource, a sphere and a checkpoint. The scene is this simple to assure intuitive interpretation of the results. The scene setup is illustrated in Figure 5. The scene setup is the same in all experiments, but the parameterization of the scene elements is varied.

- The sphere center is located at (0,0,-2) with radius 3, and has the complex refractive index of Copper. The surface is varied.
- The lightsource is a point source. Both location and spectrum are varied, but the lightsource always emits towards the “north” pole of the copper sphere at (0,0,1).
- The checkpoint is a plane located at (0,0,2.5)
- The ether is vacuum

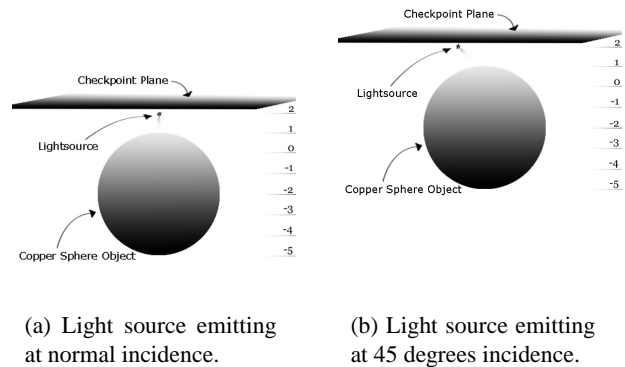


Figure 5: The test scene setup with a copper sphere component, a non-transparent checkpoint plane and a point light source.

4.1 Simulation of BRDF

The bidirectional reflection distribution function is the dependence between incident light to the reflected light. It is one of the important optical properties of a sheet of paper and the output depends strongly on the surface and subsurface representations.

The BRDF is simulated on six different configurations, one set with a diffuse surface on the copper sphere and on set with a Gaussian roughness distribution.

4.2 Totally Diffuse Surface

Four simulations were run with the copper sphere component having a totally diffuse surface SAP. A totally diffuse surface should reflect equally in all directions for any incident angle. In Figure 6 through 9 we

can see the results from the simulation with two different incident angles and two different granularities of the surface sap of the sphere.

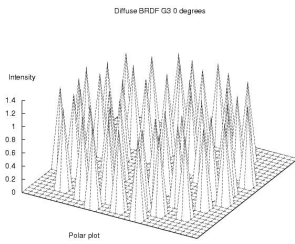


Figure 6: Incidence: 0° Granularity: 3

Illustration 6 is exactly as we would expect a totally diffuse surface BRDF to be. The deviations from this ideal case in the other three illustrations is due to two issues.

- First we can see that the 45 degrees incidents are slightly shifted towards 45 degrees reflection. This is due to the SAP being implemented as a hemisphere and not a sphere. All SAPs are rotated according to the incident angle. If the sap was a whole sphere this would have made the reflection correct for totally diffuse cases, but then one sphere would represent both reflection and transmission. This would make it impossible to rotate both according to reflection and refraction angles. The solution should then rather be not to rotate the sap (hemisphere) at all for totally diffuse surfaces, or to use a whole sphere for each of reflectance and reflectance. This correction will belong to future work for now.
- The second issue is that some of the boarder peaks in the illustrations for granularity 6, seems to have more intensity than the rest. This is probably due to the xy-plotting of latitudes. The

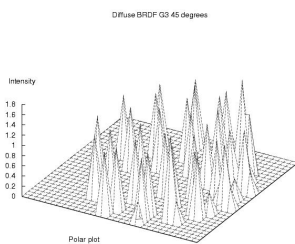


Figure 7: Incidence: 45° Granularity: 3

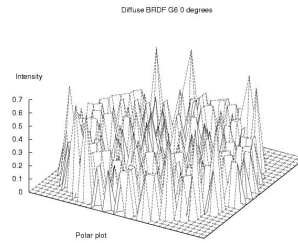


Figure 8: Incidence: 0° Granulrity: 6

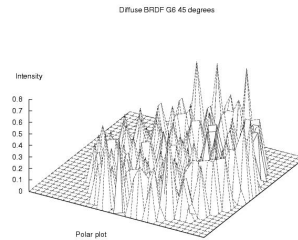


Figure 9: Incidence: 45° Granularity: 6

angles between the latitude rings are smaller in granularity 6 and at the edges more than one patch of different latitude may have been mapped to the same xy-coordinates. So this is actually a visualization problem rather than a simulation problem.

4.3 Gaussian Surface

Two simulations where run with a Gaussian distribution of the copper sphere surface roughness. The results are given in Figure 10 and 11.

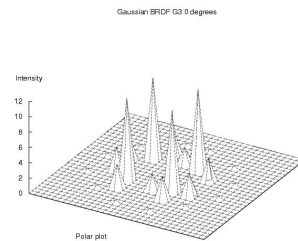


Figure 10: Incidence: 0° Granularity: 3

The expected result was a bell-shaped reflection centered at the specular direction of reflection. The illustrations of the Gaussian simulation results resembles

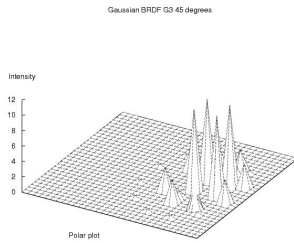


Figure 11: Incidence: 45° Granularity: 3

this shape, but the visualization is too coarse to draw conclusions. At the 45 degree incidence, the result is shifted towards specular reflection. This is according to the Gaussian distribution, but there is no intensity towards the incident angle. This is due to the same error as with the diffuse simulation.

5 Simulation of reflectance

The reflectance of copper is well known and there exist measured values of reflectance of light at normal incidence [11]. The test scene with the point source at normal incidence should be able to reproduce the measured values. The light source is setup with wavelengths for every 50nm. The rays caught by the checkpoint plane is summarized for each wavelength and visualized. The measured values taken from [11] is illustrated in Figure 13 and the simulated reflectance is given in Figure 12.

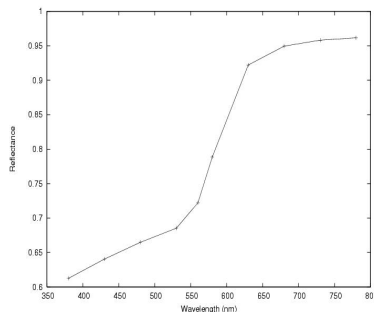


Figure 12: Simulated spectral reflectance of copper.

The correspondence between the simulated and measured reflectance is quite good. The shape of the graphs 12 and 13 are very similar, but a closer look reveals that the lower wavelengths of the simulated reflectance is a bit higher than the measured values. At

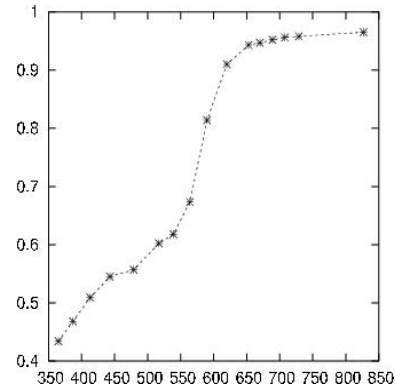


Figure 13: Measured spectral reflectance of copper.

the present time there is not possible to point at a reason for this.

6 Conclusion

The aim of this work was to develop a physically based model for light simulation in the pulp and paper industry, and to implement a prototype of this model. We have managed to develop a model in which all parts are physically described on a fairly high level of detail. However, there are still some parts of the physical foundation which may be explored further. The prototype implemented is not verifying the performance on complex structures, but the physical correctness are promising. Some issues related to the SAP implementation was revealed by the simulation results, but other solutions were suggested. The Light Propagation Model developed may serve as a foundation for physical simulation in the pulp and paper community and will hopefully inspire further exploration of its possibilities through other types of parameterization and application on more complex structures.

References

- [1] *European Synchrotron Radiation Facility*, <http://www.esfr.fr>
- [2] <http://www.acreo.se>
- [3] M. Dressen, G. Grüner, *Electrodynamics of Solids*, Cambridge University Press, 2002
- [4] Dr. E. Fred Schubert, *Refractive index and extinction coefficients of materials*, Filmetrics Corporation of San Diego, 2002 http://www.rpi.edu/~schubert/Educational/resources/Materials_refractiveindexandextinctioncoefficient.pdf

- [5] R. L. Cook, K. E. Torrance, A Reflectance Model for Computer Graphics. *ACM Transactions on Graphics*, Vol. 1, No. 1, pages: 7-24, 1982
- [6] L. Coppel, Effect of fibre length and sheet thickness on light scattering in paper - comparing measurements to Monte Carlo simulations, (A thesis, Umeaa, Sweden 2001).
- [7] K. M. Górski, B. D. Wandelt, E. Hivon, F. K. Hansen, A. J. Banday, *The HEALPix Primer*, http://www.eso.org/science/healpix/content/HEALPix_Documentation.html/intro.htm, The European Southern Observatory, 2003
- [8] P. Hanrahan, W. Krueger, *Reflection from Layered Surfaces due to Subsurface Scattering*, ACM, 1993
- [9] T. Germer, M. Nadal, Modeling the appearance of special effect pigment coatings, *Surface Scattering and Diffraction for Advanced Metrology*, page: 77-86, 2001
- [10] <http://physics.nist.gov/Divisions/Div844/facilities/scatmech/html/index.htm>
- [11] D. R. Lide, *CRC Handbook of Chemistry and Physics*, 80th edition, CRC Press, 1999
- [12] J. D. Foley, A. van Dam, S. K. Feiner, J. D. Hughes, *Computer Graphics principles and practice*, Addison-Wesley, 1990
- [13] C. A. Lindley, *Practical Ray Tracing in C*, John Wiley & sons, 1992